International Journal of Automotive Technology, Vol. 14, No. 6, pp. 971–985 (2013)
DOI 10.1007/s12239–013–0107–y

pISSN 1229–9138/ eISSN 1976–3832

MODELING AND CONTROL STRATEGY DEVELOPMENT OF A PARALLEL HYBRID ELECTRIC BUS

X. YE[1)*], Z. JIN[1)], X. HU[2), 3)], Y. LI[1)] and Q. LU[1)]

[1)]State Key Laboratory of Automobile Safety and Energy, Tsinghua University, Beijing 10084, China
[2)]National Engineering Laboratory for Electric Vehicles, Beijing Institute of Technology, Beijing 100081, China
[3)]Department of Signals and Systems, Chalmers University of Technology, Gothenburg 41296, Sweden

(Received 2 January 2013; Revised 19 February 2013; Accepted 5 March 2013)

ABSTRACT–This paper presents the system modeling, control strategy design, and experiment validation of a parallel hybrid electric bus with an automatic manual transmission (AMT) and a dry clutch. The mathematical model representation and the system architecture of the powertrain are first described. Next, a complete control scheme including energy management strategy and coordinated control of the AMT and the clutch is presented. The controller and powertrain models are then integrated in a way that the power management and the hybrid driveline perform in real world. The analysis and validation through model simulation and comparison with experiment data are conducted. A good agreement between the model and experiment demonstrates the efficacy and credibility of the integrated model. The integrated model is employed in both simulation and bench-test assessments for the development of a hybrid control unit. The results indicate that the model-based design methodology is beneficial to systematically analyzing and understanding the dynamics of hybrid electric powertrain.

KEY WORDS : Hybrid electric vehicle, Powertrain control, Energy management, Model based design

NOMENCLATURE

$\alpha_{e,cmd}$: throttle command of engine
$\alpha_{e,act}$: actual throttle of engine
ω_e : engine speed
ω_{idle} : engine idle speed
CM_e : control mode of engine
T_e : engine torque
T_m : motor torque
ω_m : motor speed
η_m : motor efficiency
P_b : battery power
$V_{b,OC}$: battery open circuit voltage
R_b : battery internal resistance
R_b : battery current
I_b : battery state of charge
x_b : battery initial state of charge
$x_{b,0}$: battery capacity
C_b : clutch position command
$P_{c,act}$: actual clutch position
γ : clutch dynamic friction torque coefficient
ω_c : speed of clutch rear disc
$\omega_{c,th}$: threshold of speed of clutch rear disc
τ_c : time constant of clutch
T_c : torque transferred through clutch
J_e : engine rotation inertia
J_m : motor rotation inertia
$T_{i,t}$: torque of transmission input shaft
$T_{t,o}$: torque of transmission output shaft
$\omega_{i,t}$: speed of transmission input shaft
$\omega_{t,o}$: speed of transmission output shaft
G_{cmd} : gear command given by HCU
G_{cur} : current gear of AMT
i_g : gear ratio of AMT
η_g : gear efficiency
F_v : joint force applied on vehicle
i_0 : gear ratio of differential
η_0 : efficiency of differential
T_b : mechanical brake torque applied on wheels
R : wheel radius
V : vehicle speed
$T_{m,EM}$: motor target torque given by energy management strategy
$T_{e,EM}$: engine target torque given by energy management strategy
C_{EM} : clutch engagement intention of energy management strategy
$G_{cmd,EM}$: gear command of energy management strategy
$\mathbf{u}$: control vector of energy management strategy
μ : equivalent factor of ECMS
T_{dem} : driver's demand torque
T^*_{dem} : driver's demand torque corresponding to the mode-switching point between EV and HEV modes

**Corresponding author.* e-mail: xiao.ye.thu@gmail.com

$T^{*}_{m,HEV}$: optimal motor torque for HEV mode
HEV : hybrid electric vehicle
HCU : hybrid control unit
BFA : backward facing approach
FFA : forward facing approach
ECMS : equivalent consumption minimization strategy
SDP : stochastic dynamic programming
DP : dynamic programing
AMT : automatic manual transmission
MBD : model based design
SOC : state of charge
CAN : controller area network
EM : energy management
CCM : coordinated control module
CEM : clutch engagement control module
GSM : gearshift control module
CTCBC : china typical city bus cycle
PI_{idle} : proportional-integral controller for engine idle speed
$PI_{spdctrl}$: proportional-integral controller for engine speed control
$f_T(\cdot)$: look-up table function for engine torque
$f_{fuel}(\cdot)$: look-up table function for engine fuel consumption rate
$f_{m,extrem}(\cdot)$: look-up table function for motor maximum and minimal torque
$f_{m,eff}(\cdot)$: look-up table function for motor efficiency
$f_{b,VOC}(\cdot)$: look-up table function for battery open circuit voltage
$f_{b,R}(\cdot)$: look-up table function for battery internal resistance
$f_{c,fric}(\cdot)$: look-up table function for battery internal resistance
$g(\cdot)$: function for battery current

1. INTRODUCTION

Hybrid electric vehicles (HEVs) technology has been recognized as a promising solution to reducing fuel consumption and air pollution for ground transportation. Academia and industry are paying more and more attention to the technology. Design and optimization of a hybrid controller is, however, challenging, because of the complexity of hybrid powertrain. In order for cost/time saving and design flexibility, model-based approach was therefore often adopted to develop control strategy for HEVs (Syed *et al*., 2006; Alt *et al*., 2010; Boukehili *et al*., 2012).

HEVs have diverse topologies, including the series, the parallel, and the series-parallel (Bayindir *et al*., 2011). This paper describes the modeling and control strategy development of a heavy-duty parallel hybrid electric city bus. Figure 1 describes the HEV powertrain configuration and its control system. This powertrain mainly consists of five sub-systems/components, namely an engine, an electric dry clutch, an electric motor (EM), a traction battery, and an automatic manual transmission (AMT). Each subsystem has its own controller, and these local controllers are connected with a hybrid control unit (HCU) through CAN (Controller Area Network) communication. General specifications of vehicle and components are listed in Table 1.

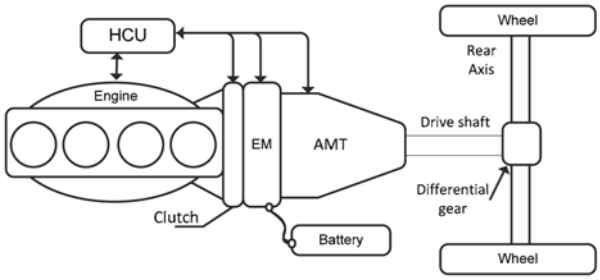

Figure 1. Powertrain architecture of the parallel hybrid electric bus.

Table 1. Vehicel parameters.

Items	Specification
Vehicle mass	15230 kg
Engine rated power	165 kW
Motor rated power	40 kW
Battery	11Ah Lithium-ion, 336 V
Transmission	6 speed AMT

The supervisory HCU is essential to ensure that all components work together to meet the driver's demand, while offering the desired fuel economy and drivability. Given driver acceleration demand and vehicle operating conditions, the HCU enables the powertrain to work around high-efficiency points by managing the power allocation between the engine and the motor, as well as by coordinating the operating status of the engine, the motor, the clutch, and the AMT.

The modeling of the powertrain is critical to design of the HCU control strategy. Various efforts have been made to develop models for hybrid electric vehicle controller design, including unified modeling (Rizzoni *et al*., 1999), bandgraphs (Filippa *et al*., 2005), and many other methods (Butler *et al*., 1999; Moore *et al*., 2006; Van Mierlo and Maggetto, 2001). Furthermore, there are commercial backward facing approaches (BFA), such as ADVISOR (Wipke *et al*., 1999; Markel *et al*., 2002; Han *et al*., 2010), and forward facing approaches (FFA), e.g., PSAT (Rousseau *et al*., 2003). BFA is suitable for optimization of energy management strategy and component sizing, but is not directly implementable for real-time control, since BFA entails a pre-defined trajectory on vehicle speed. FFA is rather causal and capable of producing online control strategy. However, commercial FFA simulation toolkits, such as PSAT, are still not well suited to provide a feasible

control strategy for an onboard HCU in reality, because dynamics of gearshift and clutch engagement is neglected. Customized modeling is thus needed for the development of a specific powertrain control.

A multitude of control strategies have been studied for energy management of hybrid electric powertrain, including rule-based (Huang *et al*., 2009; Sorrentino *et al*., 2011), fuzzy logic (Li *et al*., 2011; Shemshadi *et al*., 2010), ECMS (Delprat *et al*., 2004; Gao *et al*., 2009), SDP (Johannesson *et al*., 2007; Tate *et al*., 2010), and DP (Lin *et al*., 2003; Sundstrom *et al*., 2010). The majority of the related literature focused on power management strategy that seeks to minimize fuel consumption, while ignoring transient processes (e.g., clutch engagement and gearshift). Hence, the drivability in terms of smoothness and responsiveness of vehicle acceleration was not taken into account. Some of previous work considered the drivability by imposing penalty on clutch and gearshift events in a supervisory energy management level (Debert *et al*., 2012; Lin *et al*., 2003; Opila *et al*., 2012). Nevertheless, passenger's drive feeling is directly affected by the quality of clutch engagement and gearshift control, which can be referred to as the low-level action control or the coordinated control (He *et al*., 2012; Minh and Rashid, 2012). Although drivability is as important as fuel economy for consumers, coordinated control has attracted less attention than energy management problem in the literature.

The objective of this work is to develop a complete powertrain model and control strategy of a parallel hybrid electric bus. The powertrain model is built in accordance with a real powertrain installed on a test bench. The control strategy is developed in the simulation environment and then deployed in a microprocessor based HCU and verified on the test bench. The associated theoretical derivation and experimental validation are presented. The subsystem dynamics is carefully characterized so that the necessary transients of the powertrain can be captured, without excessive complexity. The subsystem models and the overall powertrain model architecture are introduced. Then, a sophisticated control strategy is described, which includes the energy management strategy based on ECMS, and transient-action control strategies for the clutch and the AMT. The proposed integrated powertrain-controller model is validated in both simulation and bench-test assessments. The powertrain model simulation is compared with experimental data for different driving conditions, involving some transient phenomena. The consequent results indicate a good agreement with real dynamics for both steady and transient operations of the powertrain. Fuel economy and drivability performances of the proposed controller are evaluated in a series of experiments. The powertrain-controller model can assure an in-depth analysis and understanding of the dynamics of the hybrid electric powertrain and is thus conducive to the actual development of a commercial hybrid electric city bus.

The remainder of the paper is organized as follows. In section 2, modeling of subsystems and the overall powertrain model architecture are introduced. In section 3, control strategy of the hybrid powertrain is described. The proposed powertrain-controller model is validated in section 4 followed by conclusions presented in section 5.

2. MODELING OF POWERTRAIN

The overall system architecture is first introduced in this section. Then dynamic subsystem models, including the engine model, the electric motor model, the battery model, the electric clutch model, and the AMT model, are depicted separately.

2.1. System Architecture

Matlab/Simulink tool is adopted for model development and simulations. The powertrain and vehicle models are integrated with a driver model, a test cycle model, and a HCU controller, as shown in Figure 2. Driver model generates acceleration or braking signals to track the predefined cycle speed profile. HCU interprets driver's acceleration request into torque demand, and allots the torque demand to the engine and the motor according to energy management strategy, while managing all the components to ensure smooth operation. The sophisticated clutch and AMT operations are coordinated by HCU, easing the driver manipulation. Note that brake pedal signal does not go to the HCU, since regenerative braking torque is interpreted by acceleration pedal in this study, as will be illustrated in section 3.1.2.

Figure 3 details the torque/speed flow among subsystems and the signals interacting between HCU and powertrain. Torque is delivered in a forward direction from power source to vehicle, while components speed is feedback in direction from vehicle to power source. The inputs/outputs of the subsystems are cascaded in the way demonstrated in Figure 3, while the notations corresponding to these subsystems are introduced in the following sections. The modularized architecture enables us to easily change the powertrain configuration or to replace one particular subsystem when needed. The simulation system shares the same control logic and topology of the real vehicle powertrain, and the parameters are identified by experiments to emulate the real system. The HCU algorithm developed in

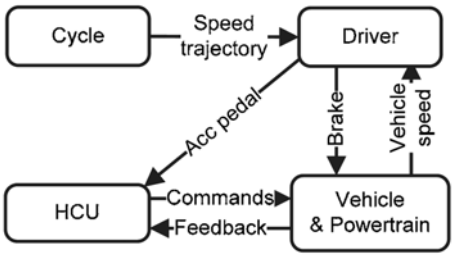

Figure 2. Top-level system architecture and control logic of simulation.

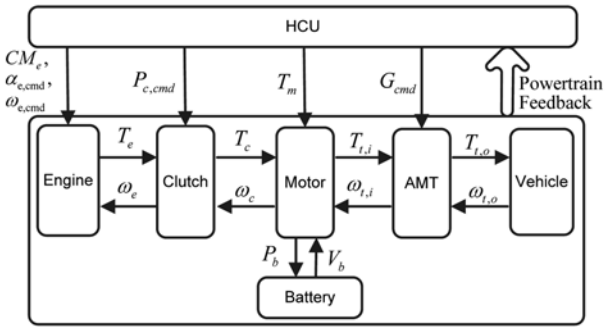

Figure 3. Powertrain model architecture and signal interactions between subsystems and HCU.

this environment can thus be directly deployed on a real-time controller and applied in practical powertrain control, leading to great convenience and significance for HCU development and parameter tuning. This is the primary motivation for proposing this modeling approach.

The subsystem models are formulated under the assumption that the drive shaft is rigid. Actually, the drive shaft is elastic, e.g., the clutch disc is equipped coil springs that aims at reducing torque jerk of the driveshaft. The rigid model and elastic model are similar for quasi-static torque input. Assuming that torque jerk is confined by coordinated control, as will be presented in Section 3.2 and Section 3.3, the proposed models are capable of representing primary dynamics of the powertrain while maintaining the succinctness of the system model.

2.2. Engine Dynamics Model

The engine modeling is essential to the powertrain modeling and can be very complicated if all the engine subsystems and dynamics are modeled (Zweiri *et al*., 2000). However, high frequency dynamics is not the primary interest of this paper, since fuel economy and drivability are mostly affected by the low frequency dynamics of powertrain. An electric injection diesel engine is adopted. The engine model is simplified such that static maps are used to characterize the engine torque output. Engine idle control and speed control logics are also presented in the model to describe the actual engine control behavior:

$$\alpha_{\mathrm{e,act}} = \begin{cases} PI_{idle}(\omega_{\mathrm{idle}} - \omega_{\mathrm{e}}), if(\omega_{\mathrm{e}} \le \omega_{\mathrm{idle}}) \\ PI_{spdctrl}(\omega_{\mathrm{e,cmd}} - \omega_{\mathrm{e}}), if(CM_e = \text{speed control}) \\ \alpha_{\mathrm{e,cmd}}, else \end{cases} \quad (1)$$

$$T_e = f_T(\alpha_{e,act}, \omega_e) \quad (2)$$

$$\dot{m}_{f,e} = f_{fuel}(\alpha_{e,act}, \omega_e) \quad (3)$$

where $\alpha_{\mathrm{e,act}}$ is the actual 'throttle' of engine. For electric injection diesel engine, there is no physical throttle; instead, the throttle value represents percentage of full load torque for given engine speed. PI_{idle} indicates output of a PI (Proportional-Integral) controller governing the engine speed ω_e to track he engine idle speed ω_{idle}. CM_e is engine control mode switching between speed control and torque control. When speed control mode of engine is activated, a PI algorithm notated as PI_{spdcrl} is performed by engine controller to follow speed command ($\omega_{\mathrm{e,cmd}}$) given by HCU; for torque control mode, engine controller responses to HCU's throttle command $\alpha_{\mathrm{e,cmd}}$, i.e., engine torque T_e and fuel rate $\dot{m}_{f,e}$, are functions of $\alpha_{\mathrm{e,act}}$ and ω_e. These two functions are presented by two-dimensional look-up tables that are obtained by bench experiments.

2.3. Electric Motor Model

Electric motor in a HEV is used to provide electric propelling power and energy recuperation for fuel economy improvement. The type of electric motor used in this study is a permanent magnet synchronous motor. The sophisticated magnetic field control is performed by an independent motor controller, namely. Hence, the focus is herein on motor external characteristics, such as maximum-minimal motor torque curves and efficiency map. The inverter loss can be combined with the electric motor loss. In this model, the desired electric motor torque is limited by a function of speed. A simple lookup table is adopted to characterize the motor-invertor efficiency depending on the motor speed and torque command. The electric motor dynamics equations are given as follows:

$$[T_{m,\min}, T_{m,\max}] = f_{m,extrem}(\omega_n) \quad (4)$$

$$T_m \in [T_{m,\min}, T_{m,\max}] \quad (5)$$

$$\eta_m = f_{m,eff}(T_m, \omega_m) \quad (6)$$

$$P_b = \begin{cases} T_m \omega_m / \eta_m, if(T_m \ge 0) \\ T_m \omega_m \eta_m, else \end{cases} \quad (7)$$

where $T_{m,\min}$ and $T_{m,\max}$ are the motor minimal and maximum torque, respectively. η_m is the motor efficiency. $f_{m,extrem}$ and $f_{m,eff}$ are look-up tables for motor torque extreme and efficiency map, respectively. P_b is the battery power.

2.4. Battery Model

Many battery models have been studied, among which the R-int model is considered as the simplest one (Johnson, 2002; Li *et al*., 2012). Note that those more complicated models, such as PNGV battery model (Nelson *et al*., 2002) and hysteresis model (Hu *et al*., 2012a, 2012b), employ more parameters to simulate the battery dynamics. However, since the modeling focus is the powertrain dynamics in a system level rather than the internal battery dynamics–a local component, we use the R-int model in which the battery open-circuit voltage and the internal resistance are delineated as a function of the battery SOC. Although the open-circuit voltage and the internal resistance are also highly related to the battery temperature, this study assumes a constant environmental temperature

for a given journey. Battery open-circuit voltage and internal resistance curves are obtained by experiments for both charging and discharging conditions. Battery dynamics are calculated by using the following equations:

$$V_{b,OC} = f_{b,VOC}(x) \tag{8}$$

$$R_b = f_{b,R}(x) \tag{9}$$

$$I_b = \frac{-V_{b,OC} + \sqrt{V_{b,OC}^2 - 4R_bP_b}}{2R_b} \tag{10}$$

$$x_b = x_{b,0} + \int_0^t \frac{I_b(t)}{3600C_b} dt \tag{11}$$

where $V_{b,OC}$ is the battery open-circuit voltage, R_b is the battery internal resistance, I_b is the battery current. x_b is the battery SOC, $x_{b,0}$ is the battery initial SOC, and C_b is the battery capacity (in ampere-hours).

2.5. Dry Clutch Model

The dry clutch functions for the purpose of gradually engaging the engine to the drivetrain while avoiding unpleasant shocks, jerks, and excessive drivetrain wear (Serrarens *et al*., 2004). In this study, the clutch is actuated by an electric motor with speed reduction rig. The command of clutch actuator position ($P_{c,cmd}$) is tracked by clutch controller by performing a closed-loop position control algorithm. Three operation states and the transition conditions are modeled in Figure 4.

In Figure 4, $P_{c,act}$ is the actuator position, $f_{c,fric}$ is the look-up-table function of friction torque, and $\gamma > 1$ is the coefficient for representing $\gamma f_{c,fric}(P_{c,act})$ as the static friction torque, since static friction force are often greater than the slip friction force under the same condition. Apart from the torque condition, a speed condition $|\omega_e - \omega_c| < \omega_{c,th}$ is required for clutch state transition from slip phase to lock phase, where ω_c is the rotating speed of clutch rear disc, and $\omega_{c,th}$ is the threshold value.

For simplicity, the clutch torque is modeled as a function of clutch actuator position in the form of a look-up table, and the torque transmitted in each state is presented by the following equation:

$$P_{c,act} = P_{c,cmd} \frac{1}{\tau_c s + 1} \tag{12}$$

$$T_c = \begin{cases} sign(\omega_e - \omega_c) \cdot f_{c,fric}(P_{c,act}) & \text{slip} \\ T_e & \text{lock} \\ 0 & \text{open} \end{cases} \tag{13}$$

where $P_{c,cmd}$ is the position command given by HCU, τ_c is the time constant of a first-order transfer function. As shown in the equations above, the clutch torques of slip phase and lock phase depend on the clutch actuator position and the engine torque, respectively.

For the clutch lock state, the engine is connected with the driveline, the engine speed is thus identical to the clutch speed.

$$\omega_e = \omega_c. \tag{14}$$

For slip phase and open phase, the engine speed is described by the following equation:

$$\omega_e(t) = \omega_{e0} + \int_{t_0}^t \frac{T_e(\tau) - T_c(\tau)}{J_e} d\tau \tag{15}$$

where ω_{e0} is the engine speed when clutch state transferred from lock to slip the last time, and t_0 is the corresponding time. J_e is the engine inertia.

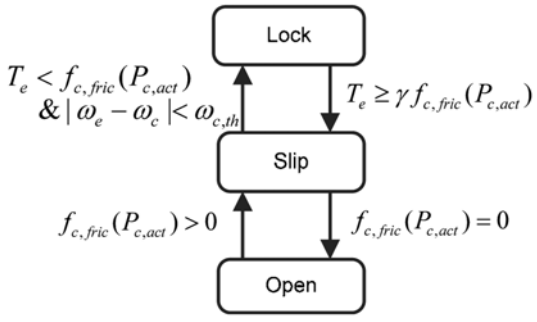

Figure 4. Clutch states and the transition conditions between them.

2.6. AMT Model

Manual transmission (MT) has the highest overall efficiency among all types of transmissions (Kluger and Long, 1999). AMT has a similar efficiency of manual transmission, since it is essentially a manual transmission with an added-on control unit that automates the shift operations (Kulkarni *et al*., 2007). The modeling of AMT emphasizes representing the AMT state transition logic and signal interacting between HCU and AMT controller, as well as the torque and speed dynamics in different states. There are three states defined in the AMT model, as shown in Figure 5. A shift process involves one loop among the three states.

In Figure 5, $T_{t,i}$ is the torque transferred through AMT input shaft, $T_{t,thresh}$ is the corresponding torque threshold under which the current gear can be disengaged. G_{cmd} is the gear command given by HCU, and G_{cur} is the current gear number. $\omega_{t,i}$ is the speed of input shaft; $\omega_{t,\text{targ}}$ is the target speed of input shaft calculated by the output shaft speed and the gear ratio of target gear; $\omega_{t,thresh}$ is the threshold under which the actuator can engage the target gear pair. In order to ensure the correct speed identification, a speed testing state is adopted to check the minimal time duration when the speed discrepancy is under threshold. t_{st} is the time instant when the speed discrepancy starts to be less than $\omega_{t,thresh}$. The dynamics of AMT depends on the gear state. For the engaged state, the AMT system can be described as

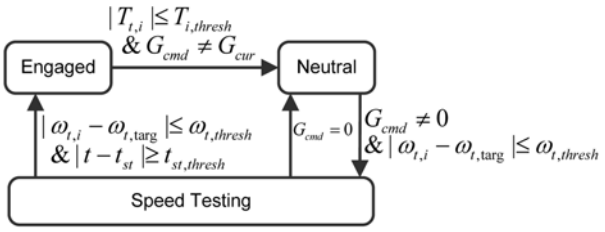

Figure 5. AMT states and the corresponding transition conditions.

$$T_{t,i} = T_c + T_m \tag{16}$$

$$T_{t,o} = T_{t,i} i_g(G_{cur}) \eta_g \tag{17}$$

$$\omega_{t,i} = \omega_{t,0} i_g(G_{cur}) \tag{18}$$

where $\omega_{t,0}$ is the speed of output shaft, $i_g(G_{cur})$ is the gear ratio of current gear number. $T_{t,o}$ is the torque of output shaft, and η_g is the gear efficiency.

The neutral state and speed testing state are actually the same physical state; their dynamics can be described by the following equations:

$$T_{t,o} = 0 \tag{19}$$

$$\omega_{t,i} = \omega_{t,i0} + \int_{t_0}^{t} \frac{T_{t,i}(\tau)}{J_{t,i}} d\tau \tag{20}$$

where $w_{t,i0}$ is the speed of input shaft when gear changed from the engaged to the neutral at the last time. $J_{t,i}$ is the lumped inertia at the input shaft, depending on the clutch status. If the clutch is engaged, then

$$J_{t,i} = J_m + J_e \tag{21}$$

else

$$J_{t,i} = J_m. \tag{22}$$

2.7. Driveline and Vehicle Model

The mathematical representations of the driveline and vehicle dynamics are described by the following equations:

$$F_v = \frac{T_{t,o} i_0 \eta_0 - T_b}{R_w} - F_{v,loss} \tag{23}$$

$$V(t) = \int_0^t \frac{F_v(\tau)}{(1+\delta) M_v} d\tau \tag{24}$$

$$\omega_{t,o} = \frac{V}{R_w} i_0 \tag{25}$$

where F_v is the joint force applied on vehicle. i_0 and η_0 are the gear ratio and efficiency of differential, respectively. T_b is the mechanical brake torque applied on wheels, and R is the wheel radius. V is the vehicle speed, δ is the rotating inertia conversion coefficient, and M_v is the vehicle mass. $F_{v,loss}$ is the vehicle resistance described by a function of the vehicle speed, the road grade, and the vehicle parameters

$$F_{v,loss} = \frac{1}{2}\rho C_d A_f V^2 + g M_v \sin(\theta) + \mu_r g M_v \cos(\theta) \tag{26}$$

where $\frac{1}{2}\rho C_d A_f V^2$ is the air drag force, ρ is the air density, C_d is the coefficient of air drag, A_f is the frontal area, and V is the vehicle speed. θ is the road grade, which is here assumed to be zero. g is the gravity unit. μ_r is rolling friction coefficient.

However, in order to better describe real vehicle resistance, a group of vehicle coast experiments were carried out to achieve the real vehicle resistance force as a function of vehicle speed, given a vehicle configuration.

$$F_{v,loss} = A_v + B_v V + C_v V^2 \tag{27}$$

where the coefficients A_v, B_v and C_v are obtained by fitting experiment data.

3. CONTROL STRATEGY FOR PHEV POWERTRAIN

The schematic control strategy is shown in Figure 6. Driver's acceleration pedal is first interpreted as torque demand, which is then split between the engine and the motor by energy management (EM) module to provide the desired engine torque $T_{e,EM}$ and motor torque $T_{m,EM}$. Clutch engagement intention (C_{EM}) can be deduced from EM module, according to

$$C_{EM} = \begin{cases} 1, & if\ T_{e,EM} > 0 \\ 0, & else \end{cases}. \tag{28}$$

Besides, a shift strategy module is adopted to generate the suitable gear command $G_{cmd,EM}$. Four commands, $T_{e,EM}$,

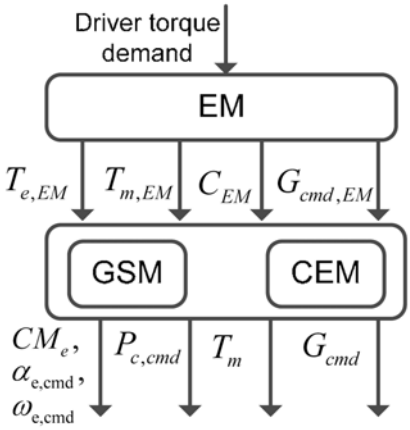

Figure 6. Schematic of powertrain control strategy.

$T_{m,EM}$, C_{EM}, and $G_{cmd,EM}$, constitute the high-level instructions of powertrain, while the low-level actions are given by coordinated control module (CCM). CCM consists of two subsystems, namely CEM and GSM, which are responsible for action control of clutch engagement and gearshift, respectively. $T_{e,EM}$ and $T_{m,EM}$ can be overwritten by CEM or GSM when necessary; $T_{e,EM}$ and $T_{m,EM}$ are directly delivered to the engine and the motor only when no transient event happens.

3.1. Energy Management Strategy

Energy management strategy involves both propelling and braking controls: for positive torque demand, propelling control splits driver's torque demand between the motor and engine; for negative torque demand, energy recuperation is managed.

3.1.1. Strategy of propelling

The Equivalent Consumption Minimization Strategy (ECMS) is the most commonly used optimization method for real-time HEV energy management application. It is considered as sub-optimal for HEV control problems, since the fuel economy deviation between ECMS and Dynamic Programming (DP, offline benchmark) was verified to be within 1% (Musardo *et al*., 2005; Kim *et al*., 2011). Hence, ECMS is chosen as the online energy management strategy in this study. The control of ECMS can be formulated by the following equation:

$$\mathbf{u}^*(t) = \underset{\mathbf{u}(t)}{\arg\min}\{P_{ef}(\mathbf{u}(t), P_{dem}(t), v(t)) - \mu^*(t) g(x(t), \mathbf{u}(t), P_{dem}(t), V(t)))\} \ . \quad (29)$$

In this paper, the term 'optimal' is employed to refer to the best solution for a given specific method and the asterisk represents the optimal solution. Here $\mathbf{u}(t) = [G_{cmd}, T_m]$ is the control solution of ECMS, where G_{cmd} is the gear command and T_m is the motor torque. $P_{dem}(t)$ is the vehicle power demand, $V(t)$ is the vehicle speed, and $P_{ef}(\mathbf{u}(t), P_{dem}(t), V(t))$ represents the fuel power consumption of Internal Combustion Engine (ICE) when $\mathbf{u}(t)$ is imposed on powertrain for vehicle power demand $P_{dem}(t)$ and vehicle speed $V(t)$. $x(t)$ is the battery SOC, and $\mu^*(t)$ is the optimal equivalent factor which converts the battery current $g(x(t), \mathbf{u}(t), P_{dem}(t), V(t))$ into equivalent fuel power consumption.

Although ECMS is more computationally efficient than DP, its implementation on real-time microprocessor still remains difficult. As shown in equation (29), optimization of ECMS requires evaluating equivalent fuel consumptions for a vector of admissible controls and choosing the one with the minimal consumption. In order to reduce the computation requirement, original ECMS controller should be simplified. First, gearshift control is simplified by extracting control strategy from the output of ECMS controller. The original and simplified gearshift maps are illustrated in Figure 7.

Then, for torque split control, an explicit solution of ECMS is adopted in this study (Ambühl *et al*., 2010). The

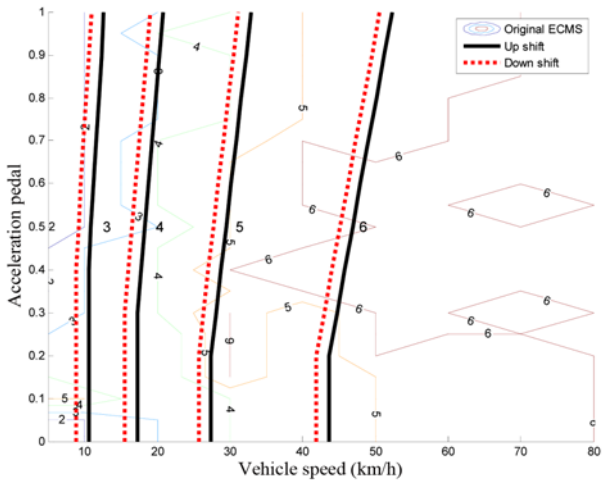

Figure 7. Gearshift map derived directly from ECMS (thin lines) and the gearshift map after regulating (thick lines).

derivation is performed by applying Willans lines models of the engine and motor models to achieve a control strategy analogous to a rule-based control, namely WL-ECMS (Willans Lines-ECMS) (Xiao *et al*., 2013). The details of WL models can be found in (Rizzoni *et al*., 1999). The WL-ECMS is determined by the following equation:

$$\begin{cases} T_{m,EM} = T_{dem} T_{e,EM} = 0 \quad if(T_{dem} < T^*_{dem}), \text{ EV mode} \\ T_{m,EM} = T^*_{m,HEV}, T_{e,EM} = T_{dem} - T^*_{m,HEV} \quad if(T_{dem} \geq T^*_{dem}), \text{ HEV mode} \end{cases} \quad (30)$$

where T^*_{dem} is the demand torque corresponding to the mode-switching point between EV and HEV modes, $T^*_{m,HEV}$ is the optimal motor torque for HEV mode. Both T^*_{dem} and $T^*_{m,HEV}$ are calculated and stored as functions of AMT input shaft speed $\omega_{t,i}$, as illustrated in Figure 8 and Figure 9, respectively.

The equivalent factor is critical for ECMS performance, but the optimal equivalent factor is difficult to be solved explicitly, since it is highly related to driving cycles that are usually unpredictable. Some algorithms about the estimation of the optimal equivalent factor were presented in (Borhan *et al*., 2012; Dac Viet *et al*., 2010; Namwook *et al*., 2012). Middle-point method is here adopted to solve the optimal μ^* as a constant for the particular cycle in offline simulation. The optimal μ^* is then employed in real-time control with a PI controller to calculate the online equivalent factor $\hat{\mu}$:

$$\hat{\mu}(t) = \mu^* + K_P[x_r - x(t)] + K_I \int_0^t [x_r - x(\tau)] d\tau \quad (31)$$

where K_P and K_I are parameters for PI controller, and x_r is the desired battery SOC reference.

The energy management strategy is organized in a two-layer structure, as described in Figure 10. The upper layer is for estimating appropriate equivalent factor $\hat{\mu}(t)$, and the lower layer for instantaneous optimization of control $\mathbf{u}(t)$

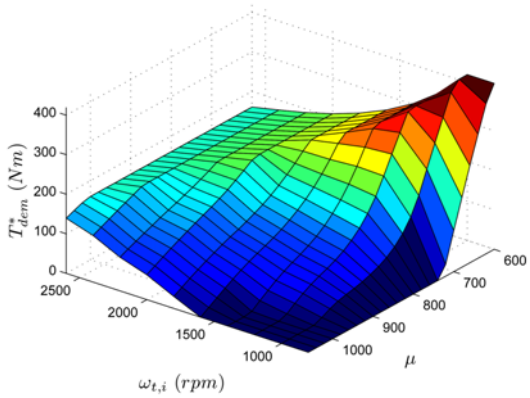

Figure 8. Demarcation torque between EV and HEV modes. Powertrain works in EV mode when driver's demand torque is below this torque, and in HEV mode when above.

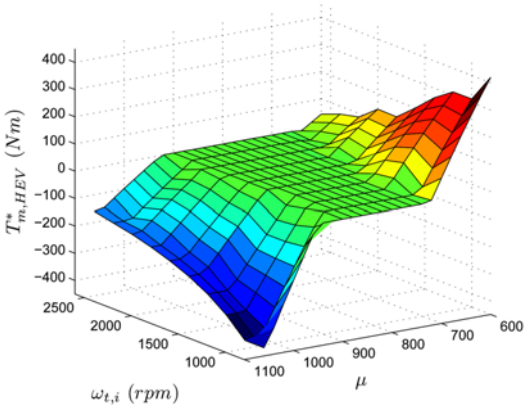

Figure 9. Optimal motor torque for HEV mode as a function of μ and ω.

by WL-ECMS, in the light of $\hat{\mu}(t)$. A similar architecture was presented in (Musardo *et al.*, 2005) as an adaptive ECMS.

3.1.2. Strategy of braking

Strategy of braking works when driver demand torque is negative. It is designed to regenerate as much energy as possible on the precondition that vehicle drivability is guaranteed.

Regenerative braking torque is interpreted by the acceleration pedal. The electric motor performs regenerative braking when the acceleration pedal is close to zero, like engine braking in conventional vehicles. Thus driver can accelerate or decelerate vehicle by manipulating the acceleration pedal. A traditional hydraulic-mechanical braking system is linked to the braking pedal. This design can simplify coordination between electric braking and mechanical braking, as well as prioritize electric braking to save more energy.

Gear shift is prohibited during electric braking, since

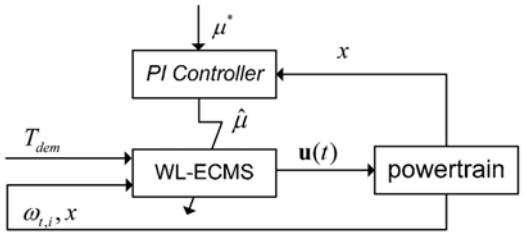

Figure 10. Structure of energy management controller.

gear shift of AMT might cause torque break in braking regeneration. It reduces the amount of energy recovered or yields a drastic torque change, thus hindering driver's brake intention and inducing uncomfortable passenger feeling. In our design, when the driver's torque demand becomes positive, the strategy allows gear change according to the propelling shift map.

3.2. Gearshift Control

No-clutch-shift control algorithm is adopted, which enables convenient shift without unnecessary clutch status change. However, it might lead to unanticipated jerks if the coordinating control strategy is designed improperly. In order to accomplish smooth torque transformation, gearshift control is subdivided into three phases, notated as phase A, B, and C, as given in Figure 11.

Phase A: This phase serves as the torque interruption buffer in gearshift control. When a gear command different from the current gear is assigned to the AMT controller, HCU ramps down the propelling torque to avoid sudden torque interruption. Besides, detaching of current gear pair can only be executed when active torque transferred through transmission is around zero. The ramping down control of propelling torque provides the time window needed for gear detaching operation. At the end of this phase, the transmission is shifted to the neutral state, and the gear engaged status is switched to 'false', which indicates the end of phase A and the start of phase B.

Phase B: Speed control is performed in this phase to

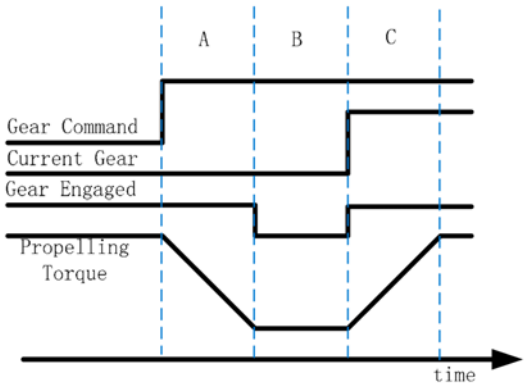

Figure 11. Sequential schematic diagram of gearshift action control.

achieve the synchronization between the transmission input and the output shaft. The speed reference ($\omega_{t,i,ref}$) is calculated by multiplying the speed of transmission output shaft ($\omega_{t,o}$) and the target gear ratio $i_g(G_{cmd})$

$$\omega_{t,i,ref} = \omega_{t,o} i_g(G_{cmd}). \quad (32)$$

The speed synchronization is performed by the electric motor, since it is more precise and faster than the engine in torque response. Moreover, in an upshift, when the speed reference is lower than current speed, the brake torque of motor will produce regenerative energy to battery, which is an additional benefit for this control method. Speed discrepancy is limited in certain range (about -20 rpm to 20 rpm) before the engagement of the oncoming gear. Then, 'gear engaged' signal is set as true, and 'current gear' as the desired gear command, denoting the control transformation from phase B to phase C.

Phase C: This phase plays the same role as phase A to prevent sudden torque change. The propelling torque ramps up at a fixed rate until it reaches the desired torque given by the energy management module. Once the desired torque is reached, the shift process is accomplished.

3.3. Clutch Control

Clutch engagement control of hybrid electric vehicles shares similarity with that of traditional AMT based powertrain (Glielmo and Vasca, 2000; Garofalo *et al*., 2001.). In this study, the idea of decoupling controller presented in (Serrarens *et al*., 2004) is adopted. Since the electric motor provides one more degree of freedom for torque control, it is used as a torque compensator to smooth the overall torque output during engagement (Hwang *et al*., 2011).

Two cases with lower and higher speeds of clutch driven plate than the engine idle speed need to be considered for clutch engagement. For the former (during vehicle launch), clutch is engaged after a slip phase, whereas for the latter (during vehicle cruise), it is possible to engage clutch with little slip. However, a compatible solution is designed for both situations. The proposed clutch engagement control is divided into 3 phases, namely A, B, and C.

Phase A: In this phase, control target is to minimize speed difference between ICE and clutch driven plate. Speed control mode is adopted to direct the engine speed to the target

$$\omega_{e,ref} = \max(\omega_{idle}, \omega_c). \quad (33)$$

The objective of phase A is accomplished if

$$|\omega_{e,ref} - \omega_e| < \omega_{c,thresh}, \quad (34)$$

where $\omega_{c,thresh}$ is the tolerance of speed difference.

Phase B: Clutch is engaged in this phase. During vehicle cruise ($\omega_c \geq \omega_{idle}$), engine is able to track the clutch speed during phase A so that clutch can be engaged as fast as possible with a negligible slip; during vehicle launch ($\omega_c < \omega_{idle}$), clutch engagement is achieved through a slip phase. The coordinated control of this slip phase is crucial since this phase is quite likely to introduce unpleasant jerk. Therefore, the theory of decoupling control is adopted, in which the engine is in speed control mode while using the motor to compensate the torque disturbance of clutch. The coordinated control of the engine, clutch actuator and motor is described as

$$\omega_{e,cmd} = \omega_{e,ref} \quad (35)$$

$$T_{c,ref} = \min[K_c(t - t_0),\ T_{e,EM}] \quad (36)$$

$$P_{c,cmd} = f_{c,fric}^{-1}(T_{c,ref}) \quad (37)$$

$$T_m = T_{dem} - f_{c,fric}(P_{c,act}) \cdot sign(\omega_e - \omega_c) \quad (38)$$

Equation (35) suggests that engine speed control mode is adopted and the reference speed is determined by equation (33). Here $f_{c,fric}(\cdot)$ represents friction torque as a function of clutch actuator position, and $f_{c,fric}^{-1}(\cdot)$ describes the target position as a function of desired clutch friction torque. Equations (36) and (37) mean that the clutch actuator position is controlled in a manner that the reference friction torque ($T_{c,ref}$) is a ramp function of time and K_c is the ramp slope. t_0 is the time when clutch begins to engage. Equation (38) denotes that the motor torque demand (T_m) is set as a compensation of torque transmitted through the clutch to meet driver's torque demand (T_{dem}), resulting in an improved drivability. These four equations define the coordinated control of the engine, the clutch, and the motor in phase B.

Phase B is finished when

$$|\omega_e - \omega_c| < \omega_{c,thresh}. \quad (39)$$

During vehicle cruise, since this condition is naturally met for clutch engagement, phase B is actually omitted, and control sequence jumps to phase C.

Phase C: In this phase, because the speed difference has already been less than the given tolerance, the remaining task is to engage clutch as rapidly as possible. The engine and motor torque commands ramp to the set points $T_{e,EM}$ and $T_{m,EM}$, respectively.

4. MODEL AND CONTROL VERIFICATION

4.1. Subsystems Validation

The subsystem parameters were first obtained on a test bench through steady-state experiments, such as efficiency map tests of the engine and the motor. Battery characteristics test was performed by a battery test bench. These parameters enable the primary study of control strategy in a simulation environment. Then, complete drive cycle tests were carried out on the test bench with the developed control strategy.

Table 2. methods for subsystem parameter verification.

No.	Component	Input (from experiment)	Simulation output	Related equations	Parameters or tables to be verified
1	Battery	I_b	V_b	$V_b = V_{OC}(x) + I_b R_b(x)$	$V_{OC}(x)$, $R_b(x)$
2	Motor & Battery	T_m ω_m	I_b	$P_b = \begin{cases} T_m\omega_m/\eta_m, if(T_m \geq 0) \\ T_m\omega_m\eta_m, else \end{cases}$	$\eta_m(T_m, \omega_m)$
		V_b		$I_b = P_b/V_b$	
3	Battery	I_b, $x_{b,0}$	x_b	$x_b = x_{b,0} + \int_0^t \frac{I_b(t)}{3600C_b}dt$	C_b
4	Engine	$a_{e,act}$, ω_e	$\dot{m}_{f,e}$	$\dot{m}_{f,e} = f_{fuel}(\alpha_{e,act}, \omega_e)$	$f_{fuel}(a_{e,act}, \omega_e)$
5	Engine	$a_{e,act}$, ω_e	$T_{t,o}$	$T_e = f_T(a_{e,act}, \omega_e)$	$f_T(a_{e,act}, \omega_e)$
	Clutch Motor AMT	$P_{c,act}$		$T_c = \begin{cases} T_e & \text{lock} \\ 0 & \text{open} \end{cases}$	$f_{c,fric}(P_{c,act})$
		T_m		$T_{t,i} = T_c + T_m$	$\eta_g(G_{cur})$
		G_{cur}		$T_{t,o} = T_{t,i} i_g(G_{cur}) \eta_g(G_{cur})$	
6	Vehicle	$T_{t,o}$	$V(t)$	$F_v = \frac{T_{t,o} i_0 \eta_0 - T_b}{R} - F_{v,loss}$	A_v, B_v, C_v
		T_b		$F_{v,loss} = A_v + B_v V + C_v V^2$	
				$V(t) = \int_0^t \frac{F_v(\tau)}{(1+\delta)M_v}d\tau$	

Real components dynamic responses are compared with their counterparts generated by simulating subsystems, given the same measured inputs. The corresponding parameters or tables are verified to ensure that the simulation output can match the experimental data. The comparison focuses on the dynamics of the engine, motor, battery, and vehicle, which affects the fuel economy performance. Due to the powertrain structure, some of the characteristics cannot be directly measured, such as the engine torque and motor torque. Instead, the torque were measured at the output shaft of AMT and compared with the corresponding torque in the simulation environment, which in turn validates the torque characteristics of the engine and the motor. The parameters and corresponding input/output of the subsystems are listed in Table 2.

China typical city bus cycle (CTCBC) was adopted on the test bench to validate the subsystems' characteristics. Plots A to C in Figures 12 and 13 illustrate a comparison between the experimental and simulated results for subsystems listed in Table 2. The corresponding analyses are presented in table 3 with the same order. These analyses include coefficients and R^2 values of the linear curve fitting for experimental and simulation data, and the standard deviation of the fitting error (*SDFE*). The coefficients a and b in table 3 represent the slope and offset in the fitting curve $Y = aX+b$, where X is experimental data, and Y is simulation data. The slope a represents the closeness between the simulation and experimental results; R^2 and *SDFE* represent dispersion of experimental data. Most of the fitting slopes and R^2 are close to 1, indicating a good match between experimental and simulation data. Although battery voltage fitting is not quite accurate, a good

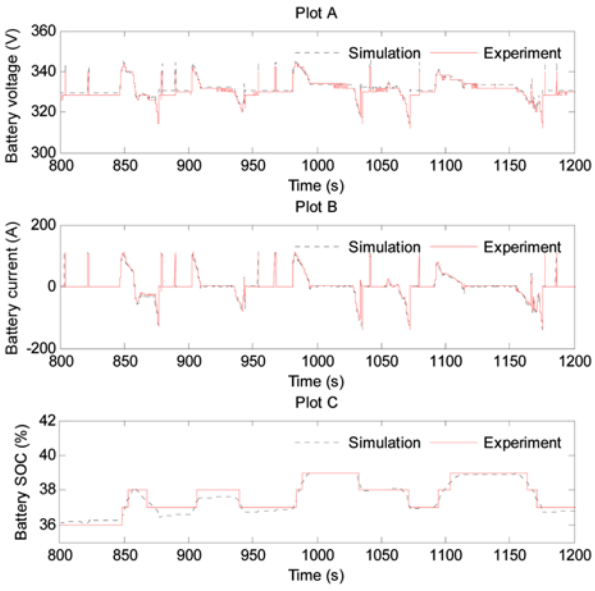

Figure 12. Battery and motor parameter validation. Plot A shows the battery voltage of simulation and experiments. Plot B depicts the battery current as a function of motor power consumption, for simulation and experiment. Plot C demonstrates the SOC trajectories of simulation and experiment.

agreement between SOC trajectories in simulation and experiment indicates the validity of the battery model in the SOC calculation, as shown in Figure 12, Plot C. Fitting for fuel consumption rate is poor, since the fuel meter is slow in dynamic response, which is incapable of representing

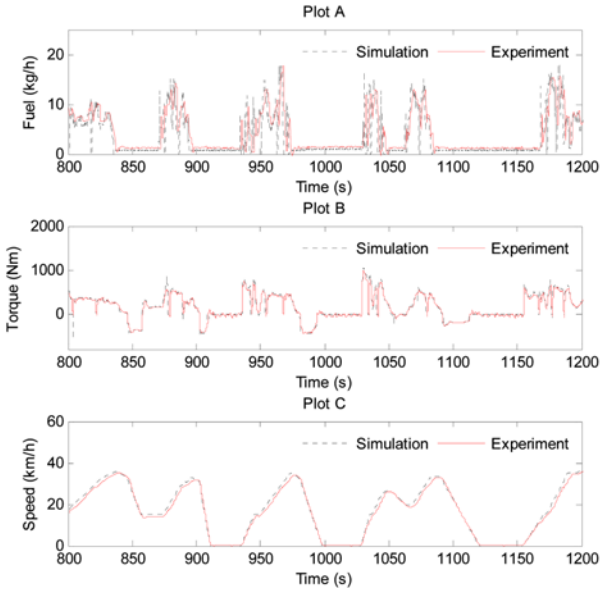

Figure 13. Subsystem dynamics comparison of experimental and simulated data for engine, motor, AMT and vehicle. Plot A shows the engine fuel rate of simulation and experiments. Plot B depicts the measured and simulated AMT output torque. Plot C demonstrates the vehicle speed trajectories of simulation and experiment.

the rapid change of engine operation. However, the overall vehicle fuel consumptions in simulation and experiment match well, as will be presented in Section 4.2.

4.2. Validation of Energy Management Strategy

4.2.1. Fuel economy comparison between traditional ECMS and WL-ECMS

Traditional ECMS (T-ECMS) using a constant equivalent factor has been verified to be a good approximation of DP (global optimum) with less than 1% deviation (Musardo *et al*., 2005, Kim *et al*., 2011). The computational advantage of T-ECMS facilitates a possible real-time application, as opposed to DP. Therefore, it can be viewed as a benchmark of real-time HEV energy control algorithm. In this study, T-ECMS and the proposed WL-ECMS are compared in terms of the vehicle fuel economy and the computational time in simulation. The results for five different cycles are shown in Table 4. The five test cycles are ECE, CTCBC, Manhattan, WVU Inter, HWFET, ranging from urban cycle to highway cycle. It is clear that WL-ECMS leads to a comparable fuel economy (merely 1.6% relative increase) with a largely shortened computational time. The observation implies that the strategy simplification involved in WL-ECMS results in a better real-time characteristic at a slight (acceptable) sacrifice of fuel economy.

Table 3. Analysis of experiment and simulation results camparasion.

Item	Linear coefficients	R^2	STDE
Battery voltage(V)	a=0.87 b=42.9	0.86	1.76
Battery current(A)	a =0.96 b=-2.0	0.94	8.53
SOC%	a =0.93 b=2.43	0.95	0.27
Fuel rate(L/h)	a=1.04 b=0.02	0.63	4.08
AMT torque(Nm)	a=0.97 b=11.51	0.91	94.7
Vehicle speed(km/h)	a=1.03 b=0.26	0.99	1.38

Table 4. Comparison between traditional ECMS (T-ECMS) and WL-ECMS.

	T-ECMS	WL-ECMS
Averaged fuel economy (L/100 km)	30.7	31.2
Relative increase	(benchmark)	1.6%
Relative computational time	(benchmark)	0.21%

4.2.2. Bench test validation

After iterative validation of subsystems, energy management strategy is developed and tuned in the simulation platform, and then compiled into C code by Simulink/Real Time Workshop (RTW). The coded algorithm is deployed in a microprocessor based HCU and validated by the bench test with a real powertrain installed. The validation is performed first by comparing the simulating and experimental curves of control signals, such as gear selection, engine throttle, and motor torque. Then statistics of cycle test, e.g., recuperated energy, motor propelling energy, and overall fuel consumption, are compared to verify the precision of the powertrain-controller model.

Plots A, B and C of Figure 14 show the comparison of the gear command, engine throttle, and motor command for a section of CTCBC test. It is clear that the commands in simulation have a good coherence with those in the bench test environment. This is because the component models are accurate, and the control strategy deployed in the bench test is the same as the one in simulation. Actually, a lot of efforts were made in the simulation environment, including tuning of shift strategy, clutch engagement strategy, and tradeoff between fuel economy and drivability. Since the interfaces of components in simulation and reality are the same, it is convenient to transfer the control program from the simulation to the real-time experiment.

Statistics of one simulation and experiment CTCBC cycle are listed in Table 5. SOC is balanced for both

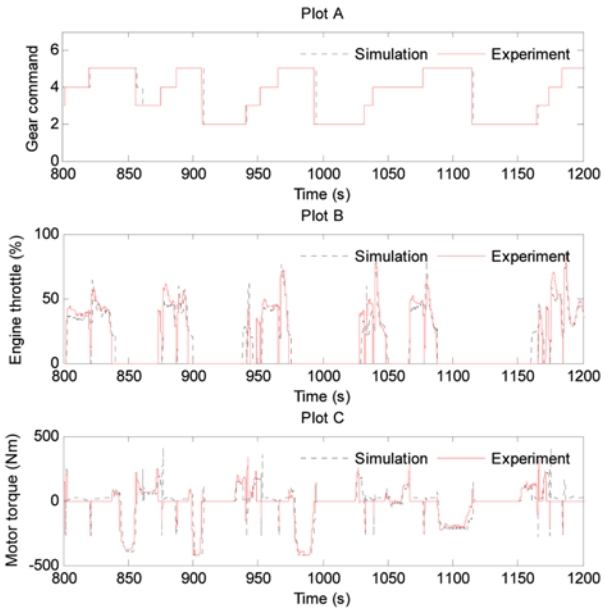

Figure 14. Control signal comparison of experimental and simulated data for AMT, engine and motor. Plot A shows the gear command. Plot B shows the engine throttle. Plot C shows the motor torque command.

simulation and experiment. All the errors are less than 5%. The fuel consumption error, which is the main concern of this study, is just 1.3%, demonstrating the precision of the powertrain model and control.

4.3. Validation of Control for Transient Actions

The transient action control of clutch engagement and gearshift is not validated by a comparison between experiment and simulation, because it is difficult to model and identify the high-frequency dynamics of real powertrain. The modeling of this study stays in such a level that the component behaviors and the transition conditions for different states are emulated. The transient action control of clutch and gear are thus validated by observing the smoothness of torque and speed transformation in the bench experiment.

Plots A, B, and C in Figure 15 illustrate the action control of gearshift with clutch engaged, which consists of three phases, as described in Section 3.2 and Figure 11. The overall shift process takes about 2 seconds, while the

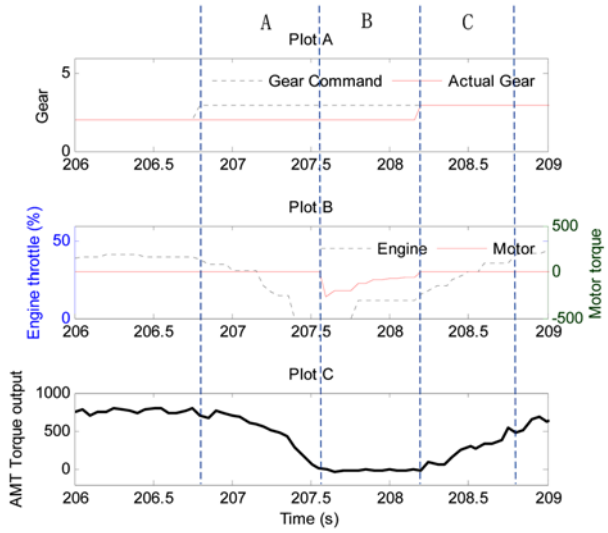

Figure 15. Action control of gearshift. Plot A shows the gear command and actual gear. Plot B shows the engine throttle and motor torque command. Plot C shows AMT output torque measured by test bench.

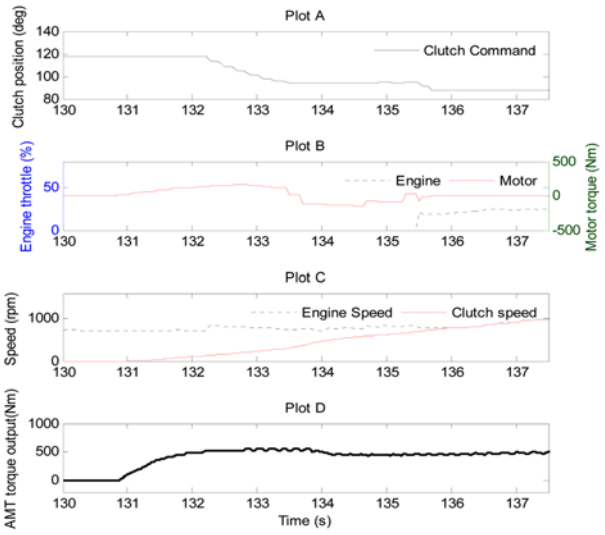

Figure 16. Action control of clutch engagement during vehicle launch. Plot A shows the clutch actuator position. Plot B shows the engine throttle and motor torque. Plot C shows the engine speed and speed of clutch driven plate. Plot D shows AMT output torque measured by test bench.

Table 5. results comparison for energy management control strategy in experiment and simulation. Test cycle is CTCBC.

Item	Simulation	Experiment	Error (%)
Fuel consumption (L/100 km)	27.6	27.95	-1.3%
Energy generated by motor (kJ)	5480	5272	4.0%
Energy stored in battery (kJ)	4626	4566	1.3%
Energy drawn from battery (kJ)	4227	4105	3.0%
Energy used in motor propelling (kJ)	3540	3490	1.4%

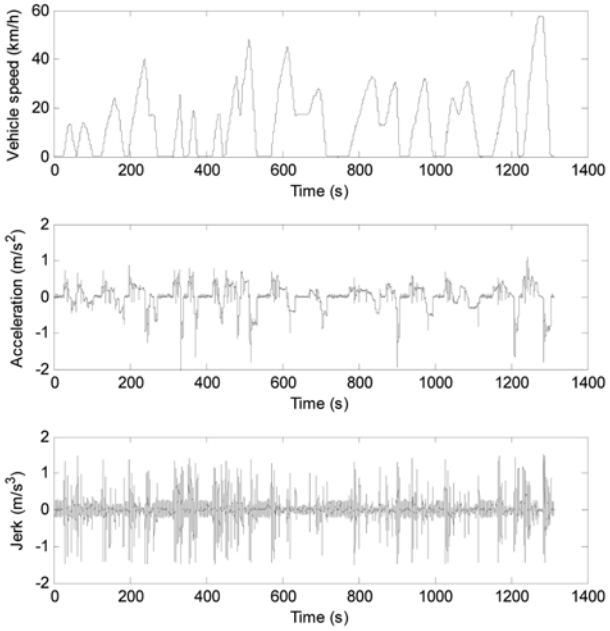

Figure 17. Vehicle speed, acceleration and jerk as functions of time for bench test, running CTCBC test cycle.

synchronization process takes about 0.6 second. The AMT torque output measured in the test bench demonstrates the smoothness of torque transformation. Despite that there are some ripples caused by engine rotation in the torque curve, they are independent of the shift process. It can be seen that no sudden torque change is induced by gearshift.

Plots A, B, C, and D in Figure 16 show the clutch engagement process in the case of vehicle launch, as a result of the control described in Section 3.3. In plot A, the clutch is completely engaged when the clutch position command is 90 degree, while being open when the clutch position is greater than 105 degree. The clutch engagement rate is controlled in a rhythm change from being fast to being slow and then becoming fast again, which is similar to the engagement pattern in control of traditional AMT dry clutch. Plot B shows the torque commands of the engine and the motor. The engine is in speed control mode during clutch slipping phase, so that no throttle command is given until the fully engagement of clutch. Plot C shows the speeds of the engine and the AMT input shaft. Plot D shows the torque of the AMT output shaft. Both Plot C and Plot D demonstrate the smoothness of clutch engagement control. The engagement process lasts for approximately 3.5 seconds. Nevertheless, the time is not constant and might alter with driver's intention.

Vehicle acceleration and jerk are often used to evaluate the vehicle performance of drivability. It is suggested that vehicle acceleration should better be confined under 1~1.5 m/s^2 for public transportation (Hoberock, 1976). Vehicle acceleration and jerk can only be calculated from vehicle speed in bench experiment. Nevertheless, calculating acceleration and jerk by differentiating the speed will inevitably incur high-frequency noise. In order to access the low-frequency vehicle dynamics, a low-pass Butterworth digital filter was applied to the acceleration and jerk signals. The sample rate was 20 Hz, and the low-pass cutoff frequency was 4 Hz. Vehicle speed, along with the calculated acceleration and jerk, **is** shown in Figure 17. It is noticed that the vehicle acceleration/deceleration is within [-2, 1] m/s^2, and vehicle jerk is within [-1.5, 1.5] m/s^3.

5. CONCLUSION

Model-based design (MBD) has been prevalent in developing control algorithms and studying behaviors of HEV powertrains. The match between the model and real components is the key of MBD approach and the main concern of this study. This paper first describes the mathematical derivation, modeling, and model architecture of a parallel hybrid powertrain. Then, a complete control strategy is introduced, which includes the energy management strategy and transient action control strategies for the clutch and AMT. The subsystems and controller, together with driving cycle and driver models, are integrated with a hierarchical methodology. The integrated model shares identical signal interfaces and control logics to those of real components, which enable comparative study and validation of simulation and bench-test experiment.

Several approaches are adopted to validate the proposed component models and control strategy. First, component dynamic responses in simulation are compared with their counterparts in the bench test, in which the model parameters are adjusted and identified to match the experimental results. Then, run-time trajectories of critical variables and qualitative statistics related to energy management strategy in simulation and experiment are compared, demonstrating that the model captures the powertrain dynamics with a good accuracy. The dynamic responses for gearshift and clutch engagement are also evaluated in the bench test, verifying its effectiveness in controlling smoothness.

It is concluded that the integrated model is effective for a systematic analysis of the powertrain operation and development of control strategy. Control strategy can thus be devised in a simulation environment and then directly deployed in a real-time controller. This design method from "simulation to production" can greatly accelerate the strategy development of HEVs, while considerably saving cost.

ACKNOWLEDGEMENT–This work was supported by The National High Technology Research and Development Program of China [Grant No. 2011AA11A206].

REFERENCES

Alt, B., Antritter, F., Svaricek, F. and Schultalbers, M. (2010). A model based control design approach for powertrain control of a parallel hybrid electric vehicle. *At-Automatisierungstechnik*, **58**, 568–579.

Ambuhl, D., Sundstr, M. O., Sciarretta, A. and Guzzella, L. (2010). Explicit optimal control policy and its practical application for hybrid electric powertrains. *Control Engineering Practice*, **18**, 1429–1439.

Bayindir, K. C., Gozukucuk, M. A. and Teke, A. (2011). A comprehensive overview of hybrid electric vehicle: Powertrain configurations, powertrain control techniques and electronic control units. *Energy Conversion and Management*, **52**, 1305–1313.

Borhan, H., Vahidi, A., Phillips, A. M., Kuang, M. L., Kolmanovsky, I. V. and Di Cairano, S. (2012). MPC-based energy management of a power-split hybrid electric vehicle. *IEEE Trans. Control Systems Technology*, **20**, 593–603.

Boukehili, A., Zhang, Y. T., Zhao, Q., Ni, C. Q., Su, H. F. and Huang, G. J. (2012). Hybrid vehicle power management modeling and refinement. *Int. J. Automotive Technology* **13**, **6**, 987–998.

Butler, K. L., Ehsani, M. and Kamath, P. (1999). A matlab-based modeling and simulation package for electric and hybrid electric vehicle design. *IEEE Trans. Vehicular Technology*, **48**, 1770–1778.

Dac Viet, N., Hofman, T., Steinbuch, M. and Serrarens, A. F. A. (2010). An optimal control-based algorithm for hybrid electric vehicle using preview route information. 2*010 American Control Conf. - ACC 2010*, *IEEE*, 5818–5823.

Debert, M., Padovani, T. M., Colin, G., Chamaillard, Y. and Guzzella, L. (2012). Implementation of comfort constraints in dynamic programming for hybrid vehicle energy management. *J. Supercritical Fluids*, **58**, 367–386.

Delprat, S., Lauber, J., Guerra, T. M. and Rimaux, J. (2004). Control of a parallel hybrid powertrain: Optimal control. *IEEE Trans. Vehicular Technology*, **53**, 872–881.

Filippa, M., Mi, C. T., Shen, J. and Stevenson, R. C. (2005). Modeling of a hybrid electric vehicle powertrain test cell using Bond graphs. *IEEE Trans. Vehicular Technology*, **54**, 837–845.

Gao, J. P., Zhu, G. M. G., Strangas, E. G. and Sun, F. C. (2009). Equivalent fuel consumption optimal control of a series hybrid electric vehicle. *Proc. Institution of Mechanical Engineers Part D-J. Automobile Engineering*, **223**, 1003–1018.

Garofalo, F., Glielmo, L., Iannelli, L. and Vasca, F. (2001). Smooth engagement for automotive dry clutch. In Decision and Control, 2001. *Proc. 40th IEEE Conf. Decision and Control. IEEE*, **1**, 529–534.

Glielmo, L. and Vasca, F. (2000). Engagement control for automotive dry clutch. *2000 American Control Conf. ACC 2000. IEEE*, **2**, 1016–1017.

Han, S. B., Chang, Y. H., Lee, E. Y., Chung, Y. J. and Suh, B. (2010). Emissions simulation in a 7000 kg-grade diesel hybrid electric vehicle. *Int. J. Automotive Technology* **11**, **1**, 105–110.

He, H. W., Liu, Z. T., Zhu, L. M. and Liu, X. L. (2012). Dynamic coordinated shifting control of automated mechanical transmissions without a clutch in a plug-in hybrid electric vehicle. *Energies*, **5**, 3094–3109.

Hoberock, L. (1976). A survey of longitudinal acceleration comfort studies in ground transportation vehicles. *J. Dynamic Systems, Measurement, and Control*, **99**, 76–84.

Hu, X., Li, S. and Peng, H. (2012a). A comparative study of equivalent circuit models for Li-ion batteries. *J. Power Sources*, **198**, 359–367.

Hu, X., Li, S., Peng, H. and Sun, F. (2012b). Robustness analysis of state-of-charge estimation methods for two types of Li-ion batteries. *J. Power Sources*, **217**, 209–219.

Huang, Y. J., Yin, C. L. and Zhang, J. W. (2009). Design of an energy management strategy for parallel hybrid electric vehicles using a logic threshold and instantaneous optimization method. *Int. J. Automotive Technology* **10**, **4**, 513–521.

Hwang, H. S., Yang, D. H., Choi, H. K., Kim, H. S. and Hwang, S. H. (2011). Torque control of engine clutch to improve the driving quality of hybrid electric vehicles. *Int. J. Automotive Technology* **12**, **5**, 763–768.

Johannesson, L., Asbogard, M. and Egardt, B. (2007). Assessing the potential of predictive control for hybrid vehicle powertrains using stochastic dynamic programming. *IEEE Trans. Intelligent Transportation Systems*, **8**, 71–83.

Johnson, V. H. (2002). Battery performance models in ADVISOR. *J. Power Sources*, **110**, 321–329.

Kim, N., Cha, S. and Peng, H. (2011). Optimal control of hybrid electric vehicles based on pontryagin's minimum principle. *IEEE Trans. Control Systems Technology*, **19**, 1279–1287.

Kim, N., Cha, S. and Peng, H. (2012). Optimal equivalent fuel consumption for hybrid electric vehicles. *IEEE Trans. Control Systems Technology*, **20**, 817–825.

Kluger, M. A. and Long, D. M. (1999). An overview of current automatic, manual and continuously variable transmission efficiencies and their projected future improvements. *SAE Trans.*, **108**, 1–6.

Kulkarni, M., Shim, T. and Zhang, Y. (2007). Shift dynamics and control of dual-clutch transmissions. *Mechanism and Machine Theory*, **42**, 168–182.

Li, K. Q., Chen, T., Luo, Y. G. and Wang, J. Q. (2012). Intelligent environment-friendly vehicles: Concept and case studies. *IEEE Trans. Intelligent Transportation Systems*, **13**, 318–328.

Li, S. G., Sharkh, S. M., Walsh, F. C. and Zhang, C. N.

(2011). Energy and battery management of a plug-in series hybrid electric vehicle using fuzzy logic. *IEEE Trans. Vehicular Technology*, **60**, 3571–3585.

Lin, C. C., Peng, H., Grizzle, J. W. and Kang, J. M. (2003). Power management strategy for a parallel hybrid electric truck. *IEEE Trans. Control Systems Technology*, **11**, 839–849.

Markel, T., Brooker, A., Hendricks, I., Johnson, V., Kelly, K., Kramer, B., O'keefe, M., Sprik, S. and Wipke, K. (2002). ADVISOR: A systems analysis tool for advanced vehicle modeling. *J. Power Sources*, **110**, 255–266.

Minh, V. T. and Rashid, A. A. (2012). Automatic control of clutches and simulations for parallel hybrid vehicles. *Int. J. Automotive Technology* **13**, **4**, 645–651.

Moore, R. M., Ramaswamy, S., Cunningham, J. M. and Hauer, K. H. (2006). A dynamic simulation tool for the battery-hybrid hydrogen fuel cell vehicle. *Fuel Cells*, **6**, 387–402.

Musardo, C., Rizzoni, G., Guezennec, Y. and Staccia, B. (2005). A-ECMS: An adaptive algorithm for hybrid electric vehicle energy management. *European J. Control*, **11**, 509–524.

Nelson, P., Bloom, I., Amine, K. and Henriksen, G. (2002). Design modeling of lithium-ion battery performance. *J. Power Sources*, **110**, 437–444.

Opila, D. F., Wang, X. Y., Mcgee, R., Gillespie, R. B., Cook, J. A. and Grizzle, J. W. (2012). An energy management controller to optimally trade off fuel economy and drivability for hybrid vehicles. *IEEE Trans. Control Systems Technology*, **20**, 1490–1505.

Rizzoni, G., Guzzella, L. and Baumann, B. M. (1999). Unified modeling of hybrid electric vehicle drivetrains. *IEEE-ASME Trans. Mechatronics*, **4**, 246–257.

Rousseau, A., Saglini, S., Jakov, M., Gray, D. and Hardy, K. (2003). Trade-offs between fuel economy and NOx emissions using fuzzy logic control with a hybrid CVT configuration. *Int. J. Automotive Technology* **4**, **1**, 47–55.

Serrarens, A., Dassen, M. and Steinbuch, M. (2004). Simulation and control of an automotive dry clutch. *American Control Conf. Proc*., **5**, 4078–4083.

Shemshadi, A., Bathaee, S. M. T., Azirani, A. A. and Kashani, S. J. (2010). Design of sugeno-type fuzzy logic controller for torque distribution in a parallel hybrid vehicle. *Int. Review of Electrical Engineering-IREE*, **5**, 536–541.

Sorrentino, M., Rizzo, G. and Arsie, I. (2011). Analysis of a rule-based control strategy for on-board energy management of series hybrid vehicles. *Control Engineering Practice*, **19**, 1433–1441.

Sundström, O., Ambühl, D. and Guzzella, L. (2010). On implementation of dynamic programming for optimal control problems with final state constraints. *Oil & Gas Science and Technology-Revue de l'Institut Français du Pétrole* **65**, **1**, 91–102.

Syed, F. U., Kuang, M. L., Czubay, J. and Ying, H. (2006). Derivation and experimental validation of a power-split hybrid electric vehicle model. *IEEE Trans. Vehicular Technology*, **55**, 1731–1747.

Tate, E. D., Grizzle, J. W. and Peng, H. E. (2010). SP-SDP for fuel consumption and tailpipe emissions minimization in an EVT hybrid. *IEEE Trans. Control Systems Technology*, **18**, 673–687.

Van Mierlo, J. and Maggetto, G. (2001). Vehicle simulation program: A tool to evaluate hybrid power management strategies based on an innovative iteration algorithm. *Proc. Institution of Mechanical Engineers Part D-J. Automobile Engineering*, **215**, 1043–1052.

Wipke, K. B., Cuddy, M. R. and Burch, S. D. (1999). ADVISOR 2.1: A user-friendly advanced powertrain simulation using a combined backward/forward approach. *IEEE Trans*. *Vehicular Technology*, **48**, 1751–1761.

Zweiri, Y. H., Whidborne, J. F. and Seneviratne, L. D. (2000). Numerical inversion of the dynamic model of a single-cylinder diesel engine. *Communications in Numerical Methods in Engineering*, **16**, 505–517.